Atomic distortion and ac-Stark shifts of H under extreme radiation conditions

M. Pont
Stichting voor Fundamenteel Onderzoek der Materie (FOM), Institute for Atomic and Molecular Physics, Kruislaan 407, 1098 SJ Amsterdam, The Netherlands
(Received 5 July 1989)

According to a general nonperturbative theory that describes atomic behavior in intense, high-frequency radiation fields, the atom becomes stable against decay by multiphoton ionization in the limit of high frequencies if the parameter $\alpha_0=(I/2)^{1/2}\omega^{-2}$ (a.u.) (with I the intensity and ω the frequency of the field) is kept constant, although otherwise unrestricted. We show that, under this condition, in the subsequent limit of strong fields (α_0 large), the Schrödinger equation describing the structure of the hydrogen atom in a laser field of circular polarization is separable in toroidal coordinates. Explicit asymptotic expressions are given for its energy eigenvalues and its eigensolutions. They correspond to a rapid decrease of the ionization potential and a drastic increase of the size of the atom with α_0. For the binding energy of the ground state we find: $|E_0|=(1/2\pi\alpha_0)(\ln\alpha_0+2.654\,284)$ (a.u.). A dramatic distortion of the shape of the atom is found, which in the strong field becomes a torus-shaped object. Furthermore, we introduce a classification of its states by strong-field quantum numbers. We show how the levels at low α_0, characterized by the weak-field quantum numbers introduced earlier, and the levels at high α_0, characterized by the strong-field quantum numbers, are correlated. We find that the energy spectrum in strong fields displays a multiplet structure. A comparison is made between our analytical results and those of a numerical calculation carried out earlier.

I. INTRODUCTION

In the domain of multiphoton ionization of atoms the phenomenon of excess-photon (above-threshold) ionization (EPI) has been known for several years now.[1] Many experiments performed in the low-frequency regime [Nd-YAG (where YAG is yttrium aluminum garnet); fundamental wavelength 1.06 μm], have involved the study of the energy spectrum of the ionized electrons (Agostini *et al.*[2] and Kruit *et al.*[3]). One of the most striking effects found was the disappearance of the low-energy part of the spectrum with increasing intensity. (The first systematic investigation of EPI was carried out by Kruit *et al.*,[3] who demonstrated the disappearance of the lowest-energy peak in the electron spectrum of Xe at an intensity of 10^{13} W cm^{-2} with pulses of 50-ps duration. Later the disappearance of the first 30 peaks in the EPI spectrum of He at an intensity of 10^{15} W cm^{-2} was reported by Lompré *et al.*[4]) A theoretical explanation of this feature was given by Muller and Tip.[5] According to these authors, the low-energy peaks are absent for low frequencies and moderately high intensities, because the decay by the associated channels is energetically forbidden due to the increase of the ionization potential of the atom in the strong laser field. The "ponderomotive effect"—caused by the spatial inhomogeneity of the intensity in the laser focus and which increases the kinetic energy of the electrons ejected from the atom as they move out—is invoked by them to explain the fact that the remaining part of the spectrum is, however, not displaced. As it turns out, in this radiation regime the ponderomotive shift almost entirely compensates the energy shift due to the increased ionization potential.

A new, yet basically unexplored, radiation regime is opened up to experiment by the advent of extremely powerful lasers. At this moment pulse intensities in excess of the atomic unit of intensity ($I_0=3.51\times10^{16}$ W cm^{-2}) can already be created in the laboratory (see, e.g., Rhodes[6]). In the near future, prospects are even more impressive.[7] Ambitious plans to construct a new generation of laser systems are now being pursued by several laboratories throughout the world.

For relatively low intensities lowest-order perturbation theory has been proven to be successful in the calculation of multiphoton transition probabilities and ac-Stark shifts (see, e.g., the book by Chin and Lambropoulos[8]). For higher intensities many higher orders in the perturbation series have to be included; eventually when the strength of the external field becomes comparable with the electrostatic forces in the atom, the series starts to diverge (see, e.g., Pan, Taylor, and Clark[9]). In fact, the above-mentioned experiments demonstrate that salient nonperturbative effects show up already at intensities well below the atomic unit. With the possibility of experimental tests in sight, the theoretical description of atomic behavior in radiation fields well beyond the atomic unit of intensity is a subject of primary fundamental interest, particularly if some underlying physical picture can be given.

Some time ago, a nonperturbative theory was developed by Gavrila and Kaminski,[10,11] especially devised to describe atomic behavior under these extreme radiation circumstances. The approach followed by these authors contrasts with the one followed by Kulander,[12] who solves the time-dependent Schrödinger equation by direct numerical integration. The Gavrila-Kaminski theory was applied to the calculation of the energy levels of a hydrogen atom in the case of a linearly polarized

laser field.[13] At fixed high frequency a dramatic decrease of the ionization potential with intensity was found. This implies that in the regime that we consider, the suppression of peaks mentioned above is absent. We predict, however, a substantial shift of the spectrum of the ejected electrons with respect to the weak-field case towards higher energies, since now the energy shift due to the altered ionization potential and the ponderomotive shift (if present[14]) act additively. The rapid decrease of the ionization potential indicates that the bound states of the atom are strongly distorted by the laser field, as opposed to radiation regimes of moderately high intensities (which have been the subject of the majority of the studies, e.g., in the experiments by Kruit *et al.*[3] and Freeman *et al.*[14]) in which only the modification of the weakly bound and continuum states plays a role. To our knowledge, no theory except the one presented by Gavrila and Kaminski takes into account the deformation of the initial state in the multiphoton ionization process. As will become apparent in the following, this effect is already important in the radiation fields produced by existing lasers, but will be even more so for the superintense lasers now being developed.

In other experiments in the low-frequency radiation regime the influence of the state of polarization of the laser field has been investigated (see Bucksbaum *et al.*[15]) and some interesting differences and similarities with the linear case studied previously have been reported. This stimulated us to study the intensity and polarization effects on the position of the energy peaks in the spectrum of EPI electrons, in our case.[16] From a numerical calculation of the levels of atomic hydrogen in a circularly polarized laser field, a decrease of the ionization potential similar to that found earlier for the case of linear polarization was obtained. We also noted the existence of certain families of states whose levels appeared to have a common asymptote in the limit of high intensities at fixed high frequency. Furthermore, in order to explore the magnitude of the deformation of the atom, averages of the radial distance were calculated. These showed a drastic increase in the size of the atom with increasing intensity. More recently we have initiated a large-scale numerical calculation of the atomic deformation of the lower-lying bound states for the case of a linearly polarized laser field over an extended range of values of intensity and frequency. This has already yielded a number of interesting features (see Pont *et al.*[17]).

In the present work we make a detailed analysis of the ac-Stark shifts and the distortion of atomic hydrogen in a combined limit of high frequency and high intensity for the circular polarization case. Among other things we will explain in detail the features just mentioned related to this polarization case.

We have organized our work as follows. In Sec. II we summarize the formalism of the multiphoton ionization theory developed by Gavrila and Kaminski. We introduce the Schrödinger equation with a "dressed" potential, which describes the structure of the hydrogen atom in the case of a photon energy high with respect to the ionization potential in the field, for the case of circular polarization. The intensity and frequency enter this equation only through the single parameter α_0. In Sec. III we discuss some features of this potential and introduce a general classification of its states. In Sec. IV we express the Schrödinger equation in the toroidal coordinate system. We solve it for the case that $\alpha_0 \rightarrow \infty$ in Sec. V. In Secs. VI and VII we discuss the physical implications of these results with regard to the deformation of the atom and the energy spectrum at high α_0. We comment on the validity and interpretation of the results of Sec. V in Sec. VIII. In Sec. IX we introduce the strong-field classification of states and establish the correlation with the states at low α_0, characterized by the weak-field quantum numbers introduced earlier. Finally, in Sec. X we make a comparison of our analytical results with those of a numerical calculation carried out earlier. We draw our conclusions in Sec. XI.

II. FORMALISM

In this section we recapitulate the results of the theory for atomic behavior in intense, high-frequency laser fields[10,11] that are of direct relevance for what follows. Its regime of validity is well understood and a number of exact numerical calculations on one-dimensional model systems have been undertaken to test it (Bardsley and Comella;[18] see also Bhatt, Piraux, and Burnett[19]).

Under certain assumptions about the laser field (dipole approximation, monochromaticity), it was shown in Ref. 11 that at sufficiently high frequencies the atom becomes stable against decay by multiphoton ionization. Its structure in the laser field is then governed by a Schrödinger equation in which the electron-nucleus attraction is replaced by a modified Coulomb potential, the "dressed potential" V_0. Thus we have for atomic hydrogen

$$[\tfrac{1}{2}\mathbf{p}^2+V_0(\alpha_0,\mathbf{r})]\Psi=E\Psi \ . \tag{1}$$

(Atomic units will be used throughout. Our results are valid for arbitrary nuclear charge by changing to Coulomb units in which lengths are expressed in the Bohr radius divided by Z and energies are expressed in hartrees times Z^2.) For the case of a circularly polarized laser field the dressed potential is given by

$$V_0=-\frac{1}{2\pi}\int_0^{2\pi}\frac{d\phi}{|\mathbf{r}+\alpha_0\hat{\mathbf{e}}_x\cos\phi+\alpha_0\hat{\mathbf{e}}_y\sin\phi|} \ . \tag{2}$$

It depends on the intensity I and frequency ω of the field through the single parameter $\alpha_0=(I/2)^{1/2}\omega^{-2}$ (a.u.). (We define the atomic unit of intensity I_0 by the time-averaged intensity corresponding to a *linearly polarized* plane wave with an electric field amplitude of 1 a.u. It amounts to $I_0=3.51\times10^{16}$ W cm^{-2}.) Here we have denoted by $\hat{\mathbf{e}}_x$ and $\hat{\mathbf{e}}_y$ the unit vectors in the x and y directions, having chosen the plane of polarization as the xy plane. The physical significance of the parameter α_0 is the classical amplitude of the oscillation of a free electron driven by the field. In Ref. 11 an iteration scheme was developed involving increasing powers of ω^{-1} to solve the exact Schrödinger equation and of which Eq. (1) represents the lowest-order approximation. To next order in the iteration the—in general complex—

"quasienergy" E attains an imaginary part, corresponding to the decay by multiphoton ionization. Expressions were derived for the (angle-dependent) n-photon ionization decay rates in which the solutions of Eq. (1) enter as initial and final states. The region of validity of the theory was found to be restricted by the requirement that the frequency of the laser field should be large with respect to the ionization potential of the ground state of the atom in the field $\omega \gg |E(\alpha_0)|$ (see Ref. 20). (We note that in the iteration scheme of the Gavrila-Kaminski theory, which proceeds in inverse powers of the frequency, the parameter α_0 is kept fixed.) The rapid decrease of the ionization potential with α_0,[16] mentioned above, greatly facilitates the satisfaction of this condition. In fact, it was shown that it can be satisfied at present laser intensities (for example, for the laser of Rhodes,[6] for which $\alpha_0 \approx 25$).

III. THE DRESSED POTENTIAL: GENERAL CLASSIFICATION OF STATES

As is easily seen from Eq. (2), V_0 is the potential due to a uniformly charged circle (of charge 1 a.u.) with radius α_0, which is centered on the origin in the plane of polarization. The dressed potential is symmetric with respect to rotations about the z axis and is also invariant under reflection in the origin. Consequently, the magnetic quantum number (m) and the parity remain good quantum numbers to describe the states of the atom in the field. Since the symmetry of our problem is in fact the same as that encountered in homonuclear diatomic molecules ($D_{\infty h}$), we adopt the standard notation of the electron terms of the latter (e.g., δ_u for states with $|m|=2$ and negative parity; it follows from symmetry considerations that the energy of the terms does not depend on the sign of m; consequently, levels with $|m| \neq 0$ are doubly degenerate).

The dressed potential V_0 is represented graphically in Fig. 1. Here we have set out the absolute value of V_0 as a function of the position in a plane, passing through the axis of symmetry. (Compare Fig. 1 of Ref. 10 for the case of the dressed potential corresponding to a linearly polarized laser field.) It is clearly shown that the modification of the Coulomb potential is such that it now attains a finite value at the origin: $-1/\alpha_0$. The two towers in Fig. 1, separated by a distance $2\alpha_0$, appear at the positions where the circle of charge passes through the base plane. This represents the fact that the dressed potential is singular at the location of the circular charge distribution. As we will prove in Sec. V, it is this (logarithmic) singularity, that dominates the high-α_0 behavior of the eigenfunctions and energies of Eqs. (1) and (2). At distances large with respect to the radius α_0 of the charged circle, the potential V_0 approaches the original Coulomb potential.

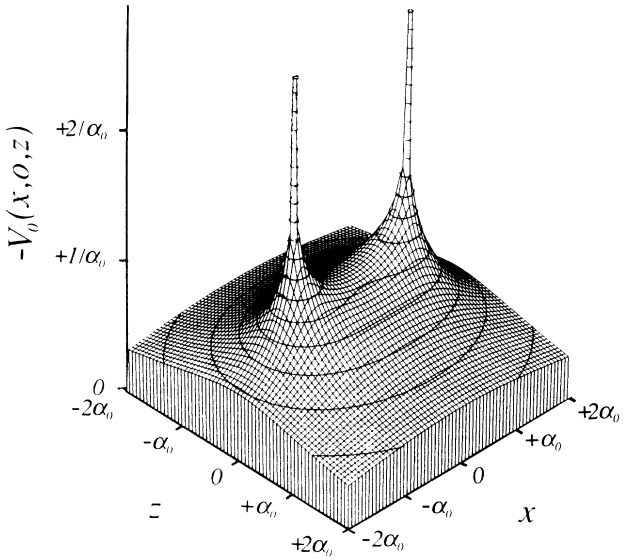

FIG. 1. The absolute value of the dressed potential for circular polarization as a function of the position in the plane through the axis of symmetry. The two logarithmic singularities appearing at the positions where the circle of charge passes through the base plane were cut off at a finite value. Note that at large distances from the circle of charge the potential approaches the original Coulomb potential as indicated by the circular contour lines.

The integral expression for V_0, Eq. (2), can be cast in a form containing an elliptic integral of the first kind K:[16,21]

$$V_0 = -\frac{2}{\pi r_+} K\left[\left[1-\left[\frac{r_-}{r_+}\right]^2\right]^{1/2}\right] . \tag{3}$$

[Compare Eq. (17) in Ref. 10 for a similar expression in the case of linear polarization.] When expressed in terms of the usual circular-cylindrical coordinates (ρ,z,ϕ) (with ρ the distance from the z axis) the quantities r_+ and r_- in Eq. (3) are given by

$$r_\pm = [(\rho \pm \alpha_0)^2 + z^2]^{1/2} . \tag{4}$$

The geometrical significance of r_+ and r_- is the largest and smallest distance from the charged circle, respectively.

Adopting circular-cylindrical coordinates and separating off the ϕ-dependent part of the full wave function Ψ in the usual way,

$$\Psi(\rho,z,\phi) = \Phi(\rho,z)\frac{e^{im\phi}}{\sqrt{2\pi}} , \tag{5}$$

the Schrödinger equation, Eq. (1), yields

$$\left[-\frac{1}{2}\left[\frac{\partial^2}{\partial\rho^2}+\frac{1}{\rho}\frac{\partial}{\partial\rho}-\frac{m^2}{\rho^2}+\frac{\partial^2}{\partial z^2}\right]-\frac{2}{\pi[(\rho+\alpha_0)^2+z^2]^{1/2}}K\left[\left[\frac{4\alpha_0\rho}{(\rho+\alpha_0)^2+z^2}\right]^{1/2}\right]\right]\Phi(\rho,z) = E\Phi(\rho,z) . \tag{6}$$

Note that the Hamiltonian appearing in Eq. (6) depends upon the magnetic quantum number m through the term $m^2/2\rho^2$. This represents the centrifugal barrier associated with the rotational motion of the electron around the z axis.

In earlier work,[16] states belonging to the same irreducible representation of $D_{\infty h}$ [i.e., having the same molecular symmetry $(\sigma_g,\sigma_u,\pi_g,\pi_u,\ldots)$] were grouped together. However, here we will adopt an alternative grouping scheme, to be explained hereafter, which is better suited to the case of present interest.

Since the Hamiltonian of Eq. (6) is symmetric in z, the wave functions fall into two classes, namely, of states symmetric and antisymmetric with respect to reflection in the xy plane. Noting that a reflection in the xy plane can be decomposed into a reflection in the origin and a rotation about 180° about the z axis, it is readily seen from Eq. (5) that $\Phi(\rho,z)$ is symmetric with respect to reflection in the xy plane for states with parity $(-1)^{|m|}(\sigma_g,\pi_u,\delta_g,\ldots)$, while it is antisymmetric for states with parity $(-1)^{|m|+1}(\sigma_u,\pi_g,\delta_u,\ldots)$.

The division into functions $\Phi(\rho,z)$ symmetric or antisymmetric with respect to reflection in the xy plane is applicable whether the parameter m in Eq. (6) is an integer or not. Increasing m in this equation continuously from the value zero, the eigenfunction $\Phi(\rho,z)$ corresponding to a $\sigma_g(\sigma_u)$ state of lowest energy develops into the eigenfunctions corresponding to the π_u, δ_g, ϕ_u, etc. (π_g,δ_u,ϕ_g) states of lowest energy, as m passes through integer values. The same applies for the state next lowest in energy, and so on.[22] This suggests the grouping together of states appearing at the same energy positions in either of the two series [i.e., $(\sigma_g,\pi_u,\delta_g,\ldots)$ or $(\sigma_u,\pi_g,\delta_u,\ldots)$]. Since the centrifugal barrier in Eq. (6) becomes more repulsive as $|m|$ increases, the energy eigenvalues of the members of each family thus formed are ordered with respect to $|m|$: $E_{\sigma_g}<E_{\pi_u}<E_{\delta_g}<\cdots$ (and similarly for $\sigma_u,\pi_g,\delta_u,\ldots$). In fact, the dependence of the energy on the magnetic quantum number of the members of a family can be expressed exactly as an integral with respect to $|m|$ over the expectation value of the inverse square of ρ:[23,24]

$$E(|m|)=E(0)+\int_0^{|m|}\langle\rho^{-2}\rangle_{|\tilde{m}|}|\tilde{m}|\,d|\tilde{m}| \ . \tag{7}$$

For the hydrogen atom in the case of high α_0 each family will appear in the spectrum as a multiplet of closely spaced levels (see Sec. VII). This special situation arises, referring to Eq. (7), whenever the average distance from the z axis is sufficiently large, such that the centrifugal barrier can be regarded as a small perturbation. The eigenfunctions $\Phi(\rho,z)$ associated with the members of a family will then be approximately equal.

IV. THE SCHRÖDINGER EQUATION IN MODIFIED TOROIDAL COORDINATES

In order to make the mathematical analysis of Eq. (6) more tractable, we adopt a coordinate system that is better adapted to the geometry of our problem than are the circular-cylindrical coordinates (ρ,z,ϕ), the toroidal coordinates (η,θ,ϕ).[25]

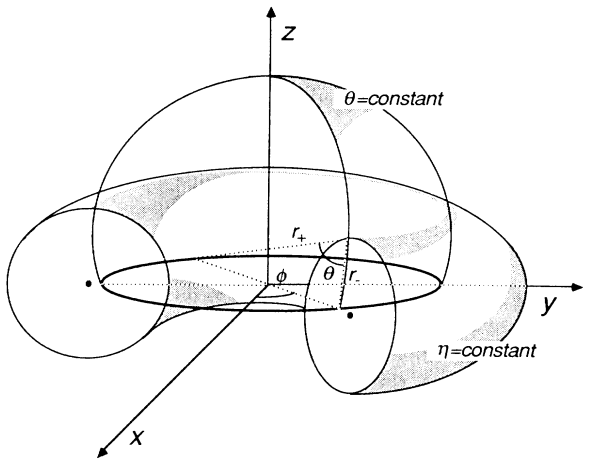

FIG. 2. The toroidal coordinates (η,θ,ϕ). The circle of charge located in the xy plane which forms the basis of this orthogonal coordinate system is indicated in the figure in boldface. The largest and shortest distance from the circle of charge is denoted by r_+ and r_-, respectively. The logarithm of the ratio between r_+ and r_- defines the coordinate η, while the angle enclosed by these two distances defines the coordinate θ. The angle ϕ is defined in the usual way.

The coordinates η and θ are defined by the logarithm of the ratio of the distances r_+ and r_-:

$$\eta=\ln(r_+/r_-) \ , \tag{8}$$

and the angle enclosed by them, respectively (see Fig. 2). The angle ϕ is defined in the usual way. Thus the surfaces of constant η are a family of tori, converging to the circular charge distribution as $\eta\to\infty$. The surfaces of constant θ are a family of spherical bowls, orthogonal to the tori and having the charged circle as a common rim. (The surfaces of constant ϕ are a family of half-planes orthogonal to both the tori and bowls.) We take θ to have positive values above the xy plane and negative values below it.

The relation to the circular-cylindrical coordinates (ρ,z,ϕ) is given by

$$\begin{aligned}\rho&=\sinh\eta/\mathcal{S} \quad (0\le\eta\le\infty) \ ,\\ z&=\sin\theta/\mathcal{S} \quad (-\pi<\theta\le\pi) \ ,\end{aligned} \tag{9}$$

with

$$\mathcal{S}=(\cosh\eta-\cos\theta)/\alpha_0 \ . \tag{10}$$

The Schrödinger equation, Eq. (6), in the toroidal coordinates (η,θ,ϕ) reads (for the derivation, see Appendix A)

$$\left[-\frac{1}{2}\left[\frac{\partial^2}{\partial\eta^2}+\frac{\partial^2}{\partial\theta^2}-\frac{(m^2-\frac{1}{4})}{\sinh^2\eta}\right]-\frac{\sqrt{2}\mathcal{S}^{-3/2}}{\pi\sqrt{\alpha_0}e^{\eta/2}}K((1-e^{-2\eta})^{1/2})\right]\tilde{\Phi}(\eta,\theta)=\mathcal{S}^{-2}E\tilde{\Phi}(\eta,\theta)\ , \tag{11}$$

where we have set

$$\tilde{\Phi}(\eta,\theta)=\rho^{1/2}\Phi(\rho,z)\ . \tag{12}$$

Note that in this system, with η as defined in Eq. (8), the argument of the elliptic function K, as appearing in the expression for the dressed potential, Eq. (3), now depends only on this single coordinate. The transformation of Eq. (12) is carried out in order to cast the Laplacian in this coordinate system in a separable form (see Ref. 25).

In order to obtain the Schrödinger equation, Eq. (11), in a form that is more suitable for further analysis we introduce a new variable r which replaces η, defined by

$$r=2\alpha_0 e^{-\eta}\quad(0\le r\le 2\alpha_0)\ . \tag{13}$$

Close to the circle of charge, r and θ have a particularly simple geometrical interpretation. In this limit the coordinate r tends to the length of the connection line to the circle of charge (denoted by $\hat{r}$) and θ tends to the angle enclosed by this line segment and the xy plane (denoted by $\hat{\theta}$) (see Fig. 3).[26] In the modified toroidal coordinates (r,θ,ϕ), we obtain from Eqs. (11) and (13) the following Schrödinger equation:

$$\left[-\frac{1}{2}\left[\frac{\partial^2}{\partial r^2}+\frac{1}{r}\frac{\partial}{\partial r}+\frac{1}{r^2}\frac{\partial^2}{\partial\theta^2}-\frac{(m^2-\frac{1}{4})}{\alpha_0^2\mathcal{Q}^2}\right]-\frac{\mathcal{P}^{-3/2}}{\pi\alpha_0}K(\mathcal{Q}^{1/2})\right]\hat{\Phi}(r,\theta)=\mathcal{P}^{-2}E\hat{\Phi}(r,\theta)\ , \tag{14}$$

where we have defined $\hat{\Phi}(r,\theta)$ by

$$\hat{\Phi}(r,\theta)=\tilde{\Phi}(\eta,\theta)=\rho^{1/2}\Phi(\rho,z) \tag{15}$$

[see Eq. (12)] and $\mathcal{P}$ and $\mathcal{Q}$ by

$$\mathcal{P}=1+\left[\frac{r}{2\alpha_0}\right]^2-2\left[\frac{r}{2\alpha_0}\right]\cos\theta\ ,\qquad \mathcal{Q}=1-\left[\frac{r}{2\alpha_0}\right]^2\ . \tag{16}$$

Note that for $\mathcal{P}$ independent of θ, the Schrödinger equation, Eq. (14), would be separable.

In order that the full wave function $\Psi(\rho,z,\phi)$ be normalized to unity, we should have

$$\int_0^{2\alpha_0}\int_{-\pi}^{\pi}|\hat{\Phi}(r,\theta)|^2\mathcal{P}^{-2}r\,dr\,d\theta=1\ , \tag{17}$$

which follows directly from the expression, Eq. (A6), of Appendix A by carrying out the substitution $\eta=-\ln(r/2\alpha_0)$.

V. DERIVATION OF THE HIGH-α_0 LIMIT

We now derive the asymptotic behavior of the eigenvalues and eigensolutions of the Schrödinger equation, Eq. (14), for large α_0. Substitution of the scaled variable

$$\xi=(\pi\alpha_0)^{-1/2}r \tag{18}$$

in the Schrödinger equation in the toroidal coordinates (r,θ,ϕ), Eq. (14), yields

$$\left[-\frac{1}{2}\left[\frac{\partial^2}{\partial\xi^2}+\frac{1}{\xi}\frac{\partial}{\partial\xi}+\frac{1}{\xi^2}\frac{\partial^2}{\partial\theta^2}\right]+\frac{2(m^2-\frac{1}{4})}{\mathcal{Q}^2}\mu^2+\mathcal{P}^{-3/2}\ln\xi+(\mathcal{P}^{-3/2}-\mathcal{P}^{-2})(\ln\mu-2\ln 2)-\mathcal{P}^{-3/2}[K(\mathcal{Q}^{1/2})+\ln\mu+\ln\xi-2\ln 2]\right]\phi_\mu(\xi,\theta)=\mathcal{P}^{-2}\varepsilon_\mu\phi_\mu(\xi,\theta)\ . \tag{19}$$

Here we have introduced

$$\mu=(\pi/4\alpha_0)^{1/2}\ , \tag{20}$$

$$\varepsilon_\mu=\frac{\pi^2}{4\mu^2}E-\ln\mu+2\ln 2\ , \tag{21}$$

and

$$\phi_\mu(\xi,\theta)=\frac{\pi}{2\mu}\hat{\Phi}\left[\xi\frac{\pi}{2\mu},\theta\right]\ . \tag{22}$$

In writing Eq. (19) in the given form we had in mind the expansion for the complete elliptic integral $K(k)$ in terms of its "complementary modulus" $k'=(1-k^2)^{1/2}$ (Ref. 21). Application of this to $K(\mathcal{Q}^{1/2})$ yields the following series in terms of $\mu\xi$:

$$K(\mathcal{Q}^{1/2})=\sum_{s=0}^{\infty}\binom{-\frac{1}{2}}{s}^2[-\ln(\mu\xi)+\psi(s+1)-\psi(s+\tfrac{1}{2})](\mu\xi)^{2s}\ , \tag{23}$$

with ψ as usual the logarithmic derivative of the Γ function $[\psi(1)-\psi(1/2)=2\ln 2]$. (Note that $\mathcal{P}$ and $\mathcal{Q}$ [see Eq. (16)] are functions of $r/2\alpha_0=\mu\xi$.)

It is thus easily seen that the limit $\mu\downarrow 0$ $(\alpha_0\to\infty)$, while keeping ξ finite, exists and yields

$$\left[-\frac{1}{2}\left[\frac{\partial^2}{\partial\xi^2}+\frac{1}{\xi}\frac{\partial}{\partial\xi}+\frac{1}{\xi^2}\frac{\partial^2}{\partial\theta^2}\right]+\ln\xi\right]\phi_0(\xi,\theta)=\varepsilon_0\phi_0(\xi,\theta)\ . \tag{24}$$

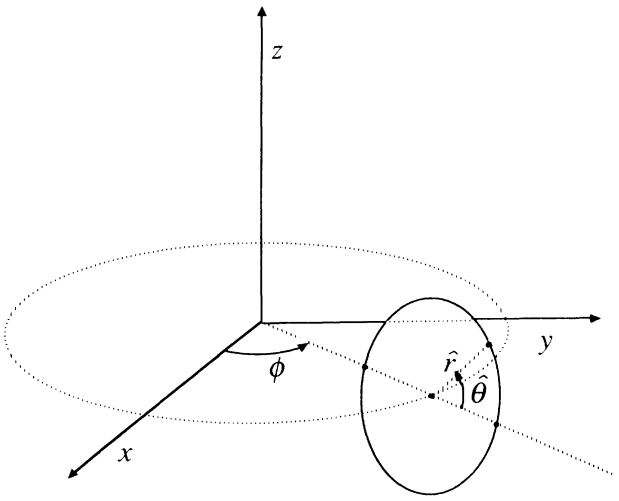

FIG. 3. The geometrical significance of the quantities $\hat{r}$ and $\hat{\theta}$ being the limiting case of the toroidal coordinates r and θ when approaching the circle of charge.

The solutions of Eq. (24) are subject to the condition of L^2 integrability:[27]

$$\int_0^{\infty}\int_{-\pi}^{+\pi}|\phi_0(\xi,\theta)|^2\xi\,d\xi\,d\theta=1\ . \tag{25}$$

Equation (24) displays that the Schrödinger equation is separable in the high-α_0 limit. Equation (24) can be solved by substitution of

$$\phi_0(\xi,\theta)=\xi^{-1/2}\chi_0(\xi)\frac{e^{i\lambda\theta}}{\sqrt{2\pi}}\ , \tag{26}$$

with λ integer.

Thus we find that χ_0 is the solution of the following one-dimensional Schrödinger equation with a logarithmic potential:

$$\left[-\frac{1}{2}\left[\frac{d^2}{dx^2}-\frac{(\lambda^2-\frac{1}{4})}{x^2}\right]+\ln x\right]\chi_0(x)=\varepsilon_0\chi_0(x)\ , \tag{27}$$

normalized in the usual way as [see Eqs. (25) and (26)]

$$\int_0^{\infty}|\chi_0(x)|^2dx=1\ . \tag{28}$$

Equation (27) is similar to the radial equation arising from spherically symmetric problems, with $|\lambda|$ ($=0,1,2,\ldots$) playing a role analogous to the azimuthal quantum number l.[28] For a given $|\lambda|$, Eq. (27) gives a set of eigensolutions, which we will specify by a generalized principal quantum number ν: $\nu=|\lambda|+k+1$, with k their number of nodes. We will adopt the same spectroscopic notation for a level characterized by ν and $|\lambda|$, as customary for the quantum numbers n and l, associated with a spherically symmetrical problem. For example, we denote the level with quantum numbers $\nu=3$ and $|\lambda|=1$ by $(3p)'$, where the prime is included to make a distinction between the two cases.

Reexpressing the solutions of Eqs. (24) and (26) in terms of the original unscaled quantities [using Eqs. (18) and (20)–(22)] yields

$$\hat{\Phi}_{\nu,\lambda}(r,\theta)=(\sqrt{\pi\alpha_0}r)^{-1/2}\chi_{\nu,|\lambda|}\left[\frac{r}{\sqrt{\pi\alpha_0}}\right]\frac{e^{i\lambda\theta}}{\sqrt{2\pi}}\ , \tag{29}$$

$$E_{\nu,|\lambda|}=\frac{1}{\pi\alpha_0}\left[-\frac{1}{2}\ln\left[\frac{\alpha_0}{\pi}\right]+\varepsilon_{\nu,|\lambda|}-3\ln 2\right]\ . \tag{30}$$

The solutions Eq. (29) are normalized [from Eqs. (22) and (25)] as

$$\int_0^{\infty}\int_{-\pi}^{\pi}|\hat{\Phi}_{\nu,\lambda}(r,\theta)|^2r\,dr\,d\theta=1 \tag{31}$$

[compare Eq. (17)].

The energy eigenvalue $E_{\nu,|\lambda|}$ and eigenfunction $\hat{\Phi}_{\nu,\lambda}(r,\theta)$ of Eqs. (29) and (30) are thus expressed in the eigenvalue $\epsilon_{\nu,|\lambda|}$ and eigensolution $\chi_{\nu,|\lambda|}(x)$ appearing in Eq. (27). Note that the wave function $\hat{\Phi}_{\nu,\lambda}(r,\theta)$ scales with α_0 in the coordinate r, but that the angular part is independent of this parameter.

Equations (29) and (30) are solutions of the Schrödinger equation [from Eqs. (18), (20)–(22), and (24)]:[29]

$$\left\{-\frac{1}{2}\left[\frac{\partial^2}{\partial r^2}+\frac{1}{r}\frac{\partial}{\partial r}+\frac{1}{r^2}\frac{\partial^2}{\partial\theta^2}\right]+\frac{1}{\pi\alpha_0}\left[\ln\left[\frac{r}{2\alpha_0}\right]-2\ln 2\right]\right\}\hat{\Phi}_{\nu,\lambda}(r,\theta)=E_{\nu,|\lambda|}\hat{\Phi}_{\nu,\lambda}(r,\theta)\ . \tag{32}$$

Equations (29) and (30) are important results, because they represent the eigenstates and energy eigenvalues of our hydrogen atom in the consecutive limits $\omega\to\infty$ and $\alpha_0\to\infty$. More precisely it is derived in Appendix B that Eq. (30) correctly gives this energy in the high-frequency limit up to order $\ln^2\alpha_0/\alpha_0^2$. The Schrödinger equation, Eq. (32), should be considered as the high-α_0 limit of the exact Eq. (14).

VI. DEFORMATION OF THE ATOM AT HIGH α_0

In this section we will discuss the physical consequences of Eq. (29). Equation (29) represents a dramatic deformation of the atom. As α_0 increases, the overall size of the atom as determined by the radius of the charged circle increases linearly with α_0. At the same time, the atom dilates uniformly and proportionally to $\sqrt{\alpha_0}$ in all directions orthogonal to the circle, i.e., in the toroidal coordinate r. This dilation as well as the decrease of the binding energy [as obtained from Eq. (30)], which accompanies it, reflects the decrease of the strength of the dressed potential with α_0. It corresponds to the decrease of the linear charge density of the circle with α_0; its charge of 1 a.u. is spread out along its periphery $2\pi\alpha_0$ (see also Sec. VIII). In particular, referring to Eq. (29), for sufficiently high α_0, the wave function will attain ap-

preciable values only inside a torus about the circle of charge, of internal radius $r_0=\sqrt{\pi\alpha_0}x_0$ and will rapidly drop to zero in all other parts of space. Here we have denoted by x_0 some value of the argument of $x^{-1/2}\chi_{\nu,|\lambda|}(x)$ beyond which this function decays rapidly to zero. Note that the atom *contracts* proportionally to $\sqrt{\alpha_0}$, if the ratio of its spreading to the radius of the charged circle is taken. We thus find that—in this relative sense—the atom localizes on the circle of charge.

In Appendix C we discuss the solutions of Eq. (27). Based on this appendix we will now discuss in some more detail the shape of the atom. In the strong-field limit, s' states of the atom (for which $|\lambda|=0$; they do not depend on θ) attain a finite value at the location of the charged circle, whereas states other than s' in contrast vanish there. As demonstrated in the Appendix, cusp behavior is absent, since the derivative of $\hat{\Phi}_{\nu,\lambda}(r,\theta)$ with respect to r vanishes as r tends to zero. For states other than s' the wave function increases as one departs from the circle as $r^{|\lambda|}$ from the value zero. The region of higher probability density of $\hat{\Phi}_{\nu,\lambda}(r,\theta)$ shifts to higher values of r as $|\lambda|$ increases, with $k(=\nu-|\lambda|-1)$ kept constant. This can be ascribed to the repulsive action of the centrifugal barrier $|\lambda|^2/2r^2$ associated with the rotational motion of the electron around the charged circle in the surface of constant ϕ. This term arises in the Hamiltonian of Eq. (32) by substitution of the angular part of $\hat{\Phi}_{\nu,\lambda}(r,\theta)$, namely, $e^{i\lambda\theta}$.

The spreading of the wave function with respect to the circle as well as the linear growth of the radius of the circle α_0 causes the amplitude of the wave function to decrease in space. In particular, it follows from Eqs. (5), (15), and (29), that for s' states, the probability density to find the particle at the location of the circle of charge decreases as α_0^{-2}.

VII. THE ENERGY SPECTRUM AT HIGH α_0

Let us now discuss the energy spectrum for the strong-field case. We found in Sec. V that the levels of the two-dimensional problem, Eq. (32) [see Eq. (29)] for $|\lambda|=0$ are nondegenerate and that the corresponding solution is symmetric with respect to reflections in the xy plane ($\theta\rightarrow-\theta$). For $|\lambda|\neq0$ the levels are doubly degenerate. By taking appropriate linear combinations [$\cos(|\lambda|\theta)$ and $\sin(|\lambda|\theta)$], we can assure that one of the two independent solutions is symmetric with respect to reflections in the xy plane and that the other is antisymmetric. We will denote the associated (normalized) wave functions by $\hat{\Phi}^{(+)}_{\nu,|\lambda|}(r,\theta)$ and $\hat{\Phi}^{(-)}_{\nu,|\lambda|}(r,\theta)$, respectively.

We also have found that the exact equation, Eq. (14), leads in the high-α_0 limit to Eq. (32), which no longer depends on the magnetic quantum number. Consequently, each level $\nu|\lambda|$ is infinitely degcnerate with respect to $|m|$. [The associated eigenstates of the hydrogen atom are obtained from Eqs. (5) and (15). This gives, for the full wave function, $\Psi(\rho,z,\phi)=(2\pi\rho)^{-1/2}\hat{\Phi}^{(\pm)}_{\nu,|\lambda|}(r,\theta)e^{im\phi}$.] The levels $|\lambda|=0$ therefore each consist of a single series of sublevels $(\sigma_g,\pi_u,\delta_g,\ldots)$ in the high-α_0 limit. The levels with $|\lambda|\neq0$ consist of two series of sublevels $(\sigma_g,\pi_u,\delta_g,\ldots)$ and $(\sigma_u,\pi_g,\delta_u,\ldots)$.

For finite α_0 the sublevels corresponding to a given pair $\nu|\lambda|$ no longer coincide. Note that at high α_0, levels corresponding to states that are symmetric with respect to a reflection in the xy plane appear in groups $(\sigma_g,\pi_u,\delta_g,\ldots)$ associated with different main levels $\nu|\lambda|$. Consequently, all states $(\sigma_g,\pi_u,\delta_g,\ldots)$ converging to some level $\nu|\lambda|$ have the same energy position in their symmetry class. Therefore, they constitute a family in the sense of Sec. III.[30] [The same applies to the antisymmetric case appearing in groups $(\sigma_u,\pi_g,\delta_u,\ldots)$.] The energy splitting between the states in such a family arising at finite α_0 can be obtained from Eq. (7). Since at high α_0 the wave functions lie about the circle of charge, we are allowed to replace $\langle\rho^{-2}\rangle$ by its lowest-order approximation $1/\alpha_0^2$.[31]

$$E(|m|)\simeq E(0)+\frac{m^2}{2\alpha_0^2}\ . \tag{33}$$

Thus we see that the splitting is indeed of higher order than the expression for the energy $E_{\nu,|\lambda|}$, Eq. (30). In this way the levels of a family are ordered with respect to the magnetic quantum number in accordance with the discussion in Sec. III.

VIII. VALIDITY AND INTERPRETATION OF THE RESULTS OF THE HIGH-α_0 LIMIT

In this section we will derive an estimate for the region of validity of the asymptotic expressions Eqs. (29) and (30) on the basis of the discussion in Sec. VI. In going from Eq. (14) to Eq. (32) we see that $\mathcal{P}$ in Eq. (14) can be replaced by unity and the elliptic integral can be replaced by the first term in the expansion, Eq. (23). Note that the term involving $\mathcal{Q}^2$ in Eq. (14) does not appear in Eq. (32). The contraction of the atom relative to the radius of the charged circle, as discussed in Sec. VI, explains why in the high-α_0 limit Eq. (32), only the behavior of the dressed potential near the location of the circle (i.e., $r\ll2\alpha_0$) is relevant. The fact that at high α_0 the wave function is concentrated in the region near the circle also explains why the Schrödinger equation is asymptotically separable. For distances close to the circle the dressed potential is invariant with respect to rotations around the circle, keeping the distance to it, r, and the polar angle ϕ constant.[32]

In going from Eq. (14) to Eq. (32) it is clear that Eqs. (29) and (30) represent approximate solutions of Eq. (14), provided $\hat{\Phi}^{(\pm)}_{\nu,|\lambda|}(r,\theta)$ has decayed sufficiently in the region where $r/2\alpha_0$ is no longer negligible with respect to 1. As a criterion of the boundary of the volume outside which the wave function drops rapidly to zero we take the surface $E=V_0(\alpha_0,\mathbf{r})$ (access to this region is classically forbidden). In the toroidal coordinates (r,θ,ϕ) this surface is determined by the equation

$$E=-\frac{\mathcal{P}^{1/2}}{\pi\alpha_0}K(\mathcal{Q}^{1/2})\ . \tag{34}$$

For α_0 high we replace E on the left-hand side by the asymptotic expression of Eq. (30) and on the right-hand side we approximate $\mathcal{P}$ by 1 and we replace the elliptic

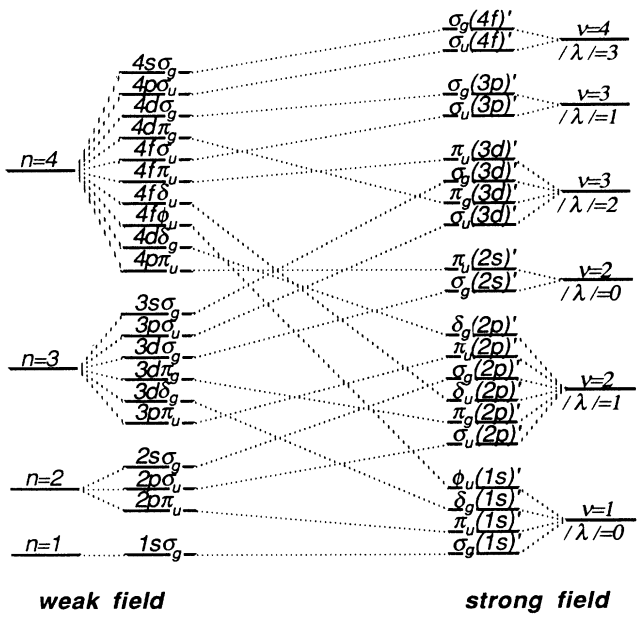

FIG. 4. Correlation diagram between levels at low α_0 (left-hand side), designated by the weak-field quantum numbers, and the levels at high α_0, designated by the strong-field quantum numbers (right-hand side). (Only the levels corresponding to $n \leq 4$ are shown.)

function K by the first term of its expansion in terms of its complementary modulus [see Eq. (23)]. Equation (34) thus yields the torus with radius

$$r_0 = \sqrt{\pi\alpha_0}\exp\varepsilon_{\nu,|\lambda|} , \tag{35}$$

valid for sufficiently high α_0.[33] We thus obtain for the region of validity of Eqs. (29) and (30), requiring $r_0 \ll 2\alpha_0$:

$$\alpha_0 \gg \exp 2\varepsilon_{\nu,|\lambda|} . \tag{36}$$

It shows that our asymptotic expressions, Eqs. (29) and (30), represent at finite values of the parameter α_0 better approximations the lower the energy of the associated state.

Let us finally comment on the interpretation of the solutions of Eqs. (32), (29), and (30). Equation (32) has a simple physical interpretation from which its relation to the original problem (i.e., that of a particle moving under the influence of a uniformly charged circle with radius α_0) becomes clear. It can be looked upon as the Schrödinger equation, corresponding to an electron moving in the potential due to a linear charge distribution of infinite extent and with density $1/2\pi\alpha_0$, expressed in circular-cylindrical coordinates with the polar axis chosen along the line of charge. (In this case the coordinate r is the distance from the polar axis and θ the polar angle.)

IX. CORRELATION OF STATES IN THE WEAK- AND STRONG-FIELD LIMITS

We now introduce the strong-field classification of the levels of our hydrogen atom by adding on the end of the molecular-spectroscopic term symbol $(\sigma_g,\sigma_u,\pi_g,\pi_u,\ldots)$ the quantum numbers ν and $|\lambda|$ of the main level at which each of the individual levels converges [e.g., $\delta_u(2p)'$ designates the state with $|m|=2$ and negative parity, which converges in the high-α_0 limit to the level with quantum numbers $\nu=2$ and $|\lambda|=1$]. Note that this classification determines the levels uniquely, since not more than one level of a certain species $(\sigma_g,\sigma_u,\pi_g,\pi_u,\ldots)$ converges to a certain level with to quantum numbers ν and $|\lambda|$ in the strong-field limit.

A unique correspondence can be made between the levels at high α_0, designated by the strong-field quantum numbers, introduced above and the levels at low α_0, designated by the weak-field quantum numbers, introduced earlier (see Ref. 16). The weak-field quantum numbers are obtained by adding in front of the molecular-spectroscopic term symbol the principal quantum number n and the azimuthal quantum number l of the state from which it develops continuously in the low-α_0 limit (e.g., $3p\pi_u$ designates the state with $|m|=1$ and negative parity, which develops in the weak-field limit from the unperturbed hydrogenic state with $n=3$ and $l=1$). Note that the weak- and strong-field classifications of levels are defined in analogy with the united-atom limit and the separated-atom limit of (one-electron) homonuclear diatomic molecules.

The ordering of the sublevels, corresponding to a certain principal quantum number, at low α_0 (left-hand side of Fig. 4) can be obtained from perturbation theory for the Coulomb potential [see Eqs. (24)–(27) of Ref. 16], to which the dressed potential tends in the weak-field limit. The ordering of the sublevels which correspond to a certain pair of quantum numbers ν and $|\lambda|$ at high α_0 (right-hand side of Fig. 4) is immaterial for the actual correlation. [As will become apparent in the next paragraph, this is because, as we have seen, not more than one level of a certain species $(\sigma_g,\sigma_u,\pi_g,\pi_u,\ldots)$ converges to a certain level with quantum numbers ν and $|\lambda|$.] Nevertheless, we have ordered the states within each family (in the sense of Sec. III), i.e., with respect to the magnetic quantum number. The ordering of the main levels $\nu|\lambda|$ [see Eq. (30)] is obtained from Table I of Appendix C. In order of increasing energy we have $(1s)'$, $(2p)'$, $(2s)'$, $(3d)'$, $(3p)'$, $(3p)'$, $(4f)'$, ...

The correlation can now be established, as shown schematically in Fig. 4 by the connecting lines, by the Wigner–von Neumann "noncrossing rule."[22] Since the parity and the z component of the angular momentum are conserved at all α_0, two separate states having the same molecular symmetry (belonging to the same irreducible representation of $D_{\infty h}$) cannot cross, as the parameter α_0 is varied. Thus the lowest σ_g state on each side is correlated with each other, then the next-lowest pair, and so on; the same holds for the other symmetries $(\sigma_u,\pi_g,\pi_u,\ldots)$. Note that crossings of states having different symmetries are not forbidden and occur frequently in Fig. 4.

The weak-field classification of states lowest and next lowest in energy of a species $(\sigma_g,\sigma_u,\pi_g,\pi_u,\ldots)$ can be easily derived directly from the spectrum of the Coulomb potential. One thus finds that for families of states of

lowest or next-lowest energy in either series $(\sigma_g,\pi_u,\delta_g,\ldots)$ or $(\sigma_u,\pi_g,\delta_u,\ldots)$ every next member in the family has a principal quantum number n and an azimuthal quantum number l, which is one higher than its predecessor. For example, the family of states next lowest in energy in the series $(\sigma_g,\pi_u,\delta_g,\ldots)$ concerns $2s\sigma_g$, $3p\pi_u$, $4d\delta_g$, $5f\phi_u,\ldots$. However, for the families of states associated with an energy position higher than 2, the situation is more complex, because here the l degeneracy of the Coulomb potential plays a role. To obtain the appropriate l quantum number it is necessary to know how the unperturbed Bohr level splits up in weak fields [see Eqs. (24)–(27) of Ref. 16; it was used in the correlation diagram Fig. 4]. The assignation of a principal quantum number to the levels follows the same rule as above: it increases with unity for every next member in the family.

To gain some insight into how wave functions in the weak-field limit develop into the wave functions in the strong-field limit it is useful to investigate the location and shape of nodal surfaces in these two limiting cases. Let us consider the states of lowest energy in the series $(\sigma_g,\pi_u,\delta_g,\ldots)$: $1s\sigma_g$, $2p\pi_u$, $3d\delta_g$, $4f\phi_u,\ldots$. From the correlation diagram we find that this family converges in the strong-field limit to the level denoted by $(1s)'$. Note that neither in the weak-field limit nor in the strong-field limit have the wave functions any nodal surfaces,[34] which suggests their absence at all α_0.

Let us consider next the states of lowest energy in the series $(\sigma_u,\pi_g,\delta_u,\ldots)$, $2p\sigma_u$, $3d\pi_g$, $4f\delta_u$, $5g\phi_g,\ldots$, and the states next lowest in energy in the series $(\sigma_g,\pi_u,\delta_g,\ldots)$, $2s\sigma_g$, $3p\pi_u$, $4d\delta_g$, $5f\phi_u,\ldots$, for $n\leq 4$. According to the correlation diagram these two families converge to the same asymptote: the level denoted by $(2p)'$. Note that the states of the antisymmetric family have the xy plane as a nodal surface. This is also the only nodal surface in the low-α_0 limit. In the high-α_0 limit, as determined by the vanishing of $\sin\theta$, the wave functions vanish for $\theta=0$ (the xy plane for $\rho>\alpha_0$) and $\theta=\pi$ (the xy plane for $\rho<\alpha_0$), thus again yielding the xy plane. In the symmetric case we deal with a spherical nodal surface in the low-α_0 limit. The position of nodal surfaces in the high-α_0 limit is determined by the vanishing of $\cos\theta$. Now the surfaces $\theta=\pi/2$ and $\theta=-\pi/2$ constitute together also a spherical nodal surface (for $z>0$ and $z<0$ respectively; see also Fig. 2), now passing through the circle of charge.[35] This suggests that no nodal surfaces other than of the given type are present at intermediate α_0. A similar conclusion about the occurrence of nodal surfaces can be drawn for the family $3p\sigma_u$, $4d\pi_g$, $5f\delta_u$, $6g\phi_g,\ldots$, converging at the level $(3d)'$.

X. COMPARISON WITH NUMERICAL RESULTS

In this section we will make a comparison of the results of our analysis with the numerical calculation of Ref. 16 carried out within the framework of the "decoupled l-channels approximation." We will first discuss the sizes of the atom and subsequently discuss the energies of the levels.

In Ref. 16 we calculated the averages of the radial distance $\bar{r}$ for states corresponding to principal quantum number $n\leq 4$. We found for sufficiently high α_0, a linear relationship between $\bar{r}$ and α_0 with a slope of roughly 1. From this linearity and from the scaling law that relates $\bar{r}$ for atomic hydrogen to the case of arbitrary nuclear charge Z [see Eq. (30) of Ref. 16], it is readily shown that this quantity is independent of Z for sufficiently large α_0. Thus the size of the atom depends on the shape and size of the dressed potential as determined by α_0 rather than its overall strength Z. This is in agreement with the present analysis, which shows that for sufficiently high α_0 the atom has the shape of a torus, the external radius of which equals α_0.[36]

We will now make a comparison between our present results for the energies of the levels and the numerical results in Ref. 16. Let us consider the states of lowest energy in the series $(\sigma_g,\pi_u,\delta_g,\ldots)$, $1s\sigma_g$, $2p\pi_u$, $3d\delta_g$, $4f\phi_u,\ldots$. In Fig. 5 we have given those levels corresponding to $n\leq 4$, calculated by the method of Ref. 16. As we predicted in Sec. VII, levels belonging to the same family converge at high α_0. It is clearly displayed, that this is indeed the case in Fig. 5. From the correlation diagram, Fig. 4, we find that this family converges to the level denoted by $(1s)'$.

In Fig. 6 a comparison is made for the ground state $1s\sigma_g[=\sigma_g(1s)']$ between the asymptotic formula Eq. (30) for $E_{\nu=1,|\lambda|=0}$ (with $\varepsilon_{\nu=1,|\lambda|=0}$ obtained from Table I of Appendix C) with the numerical result of Ref. 16. Excellent agreement is obtained up to quite low values of α_0. The agreement is even better than one may expect on the basis of the estimate, Eq. (36). [Any discrepancy between the analytical (dashed) curve and the calculated (solid) curve at high α_0 is very likely to be ascribed to the fact that we deal here in fact with a "decoupled l-channels approximation" (see Ref. 16), which we know to become worse as α_0 becomes large.]

In Fig. 7 a comparison between the analytical and calculated curves is given for the other states appearing in Fig. 5, $2p\pi_u(1s)'$, $3d\delta_g(1s)'$, and $4f\phi_u(1s)'$. Here we have taken into account the effect of the centrifugal barrier by simply adding $m^2/2\alpha_0^2$ to the formula Eq. (30) [in accordance with Eq. (33)]. Extrapolation of their asymptotes suggests that indeed the levels with $|m|=1$, 2, and 3 originating from the $(1s)'$ level at high α_0, are connected to the unperturbed hydrogenic states with $n=2$, 3, and 4 in the low-α_0 limit.

In Fig. 8 we have displayed the states of lowest energy in the series $(\sigma_u,\pi_g,\delta_u,\ldots)$, $2p\sigma_u$, $3d\pi_g$, $4f\delta_u$, $5g\phi_g,\ldots$, and the states next lowest in energy in the series $(\sigma_g,\pi_u,\delta_g,\ldots)$, $2s\sigma_g$, $3p\pi_u$, $4d\delta_g$, $5f\phi_u,\ldots$, for $n\leq 4$. For all three families shown so far in Figs. 5 and 8, we find that levels within a family are ordered with respect to their magnetic quantum number (as predicted in Sec. III). A typical difference with the former case, Fig. 5, is that now in Fig. 8 two families (of states symmetric and antisymmetric with respect to reflections in the xy plane) converge with the same asymptote, the level denoted by $(2p)'$ (see the correlation diagram Fig. 4). This is in accordance with the discussion in Sec. VII,

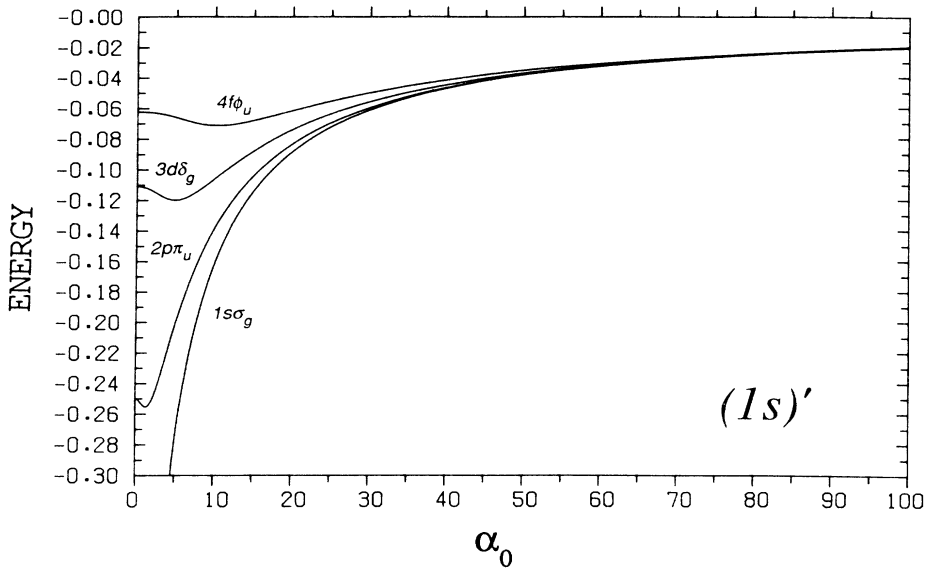

FIG. 5. The family of states of lowest energy in the series $(\sigma_g, \pi_u, \delta_g, \ldots)$ for $n \leq 4$, $1s\sigma_g$, $2p\pi_u$, $3d\delta_g$, $4f\phi_u$, as obtained from numerical calculation (see Ref. 16). Energies are expressed in Rydberg units.

where we showed that for a main level of s' type, there is only one corresponding family, whereas each main level that is not of the s' type has two families associated with it.

XI. CONCLUSIONS

We have considered the structure of the hydrogen atom in a circularly polarized laser field, as described by a "dressed" potential if the photon energy becomes large with respect to the ionization potential. We have shown that this Schrödinger equation is separable in the toroidal coordinate system as $\alpha_0 \to \infty$. Explicit expressions are given for its energy eigenvalues and its eigensolutions. They correspond to a drastic reduction of the ionization potential and a dramatic deformation of the atom. For the ground-state energy we find

$$E_0 = \frac{1}{\pi\alpha_0}\left[-\frac{1}{2}\ln\left[\frac{\alpha_0}{\pi}\right]+\varepsilon_0-3\ln 2\right],$$

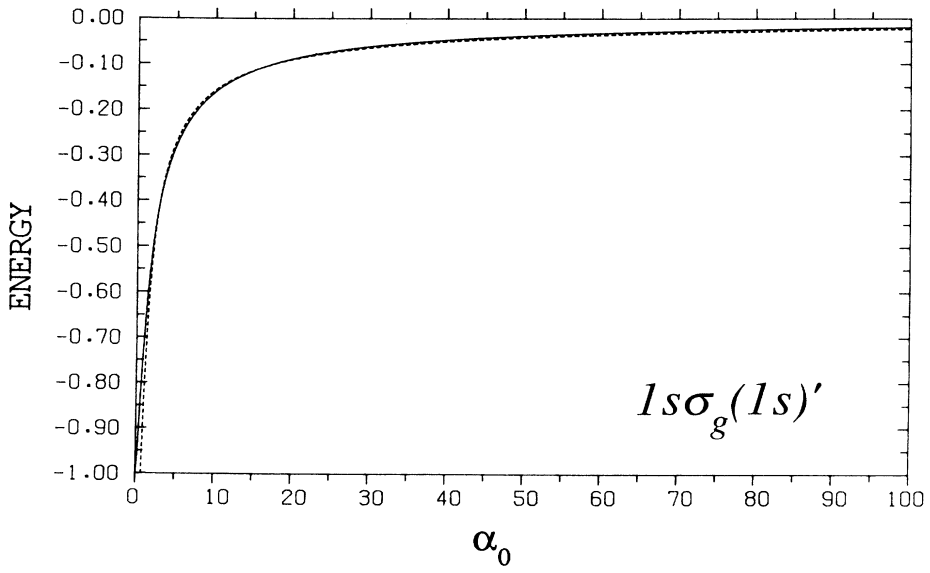

FIG. 6. Comparison of the analytical formula, Eq. (30), with $\varepsilon_{\nu,|\lambda|}$ given by Table I, with the numerical result of Ref. 16 for the ground state of atomic hydrogen $1s\sigma_g(1s)'$. Energies are expressed in Rydberg units.

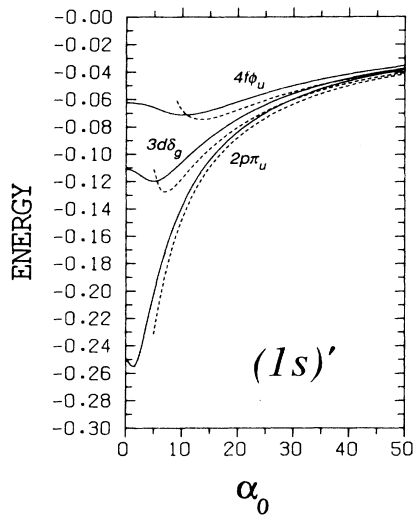

FIG. 7. Same as in Fig. 6 for the other states of the family $1s\sigma_g$, $2p\pi_u$, $3d\delta_g$, $4f\phi_u$, . . . , for $n \leq 4$. Here we have included the effect of the centrifugal barrier by simply adding $m^2/2\alpha_0^2$ to the result of Eq. (30) in accordance with Eq. (33).

with ε_0 the lowest-energy eigenvalue of a Schrödinger equation with a logarithmic potential ($\varepsilon_0 = 0.179\,935$). The atom in the strong field becomes a torus-shaped object. As a result of the separability new quantum numbers arise analogous to the principal quantum number and the azimuthal quantum number in spherically symmetric problems: the strong-field quantum numbers ν and $|\lambda|$. It turns out that each level associated with a pair of strong-field quantum numbers is in fact (infinitely) degenerate. At high but finite α_0 each main level splits up into one or two multiplets, which we refer to as families. If only one family appears, it consists of states that are symmetric with respect to a reflection in the xy plane. In the other case, the second family consists of states antisymmetric with respect to a reflection in the xy plane. We have also shown that each family consists of states having the same energy position in either of the series $(\sigma_g, \pi_u, \delta_g, \ldots)$ or $(\sigma_u, \pi_g, \delta_u, \ldots)$. The members of each family are ordered with respect to the magnetic quantum number, such that the higher the $|m|$, the higher the energy, which is due to the repulsion of the centrifugal barrier associated with the rotational motion about the symmetry axis of the charged circle. We have established the correlation between the states at low α_0, characterized by the weak-field quantum numbers introduced earlier and the strong-field quantum numbers introduced here. A practical condition of applicability of our asymptotically exact expressions at finite but high α_0 is derived. A comparison of our analytical results with a numerical calculation carried out earlier shows excellent agreement up to rather low values of α_0. Our findings apply to the radiation fields of already existing lasers and should play a major role in the understanding of the behavior of atoms in the fields produced by the extremely powerful lasers now being developed. Angular-dependent ionization rates on the basis of the Gavrila-Kaminski expression (obtained in the next order in the iteration in the inverse frequency) are now being computed. An extension of the present analysis for circular polarization to the case of a linearly polarized laser field proceeding along similar lines is also in progress.

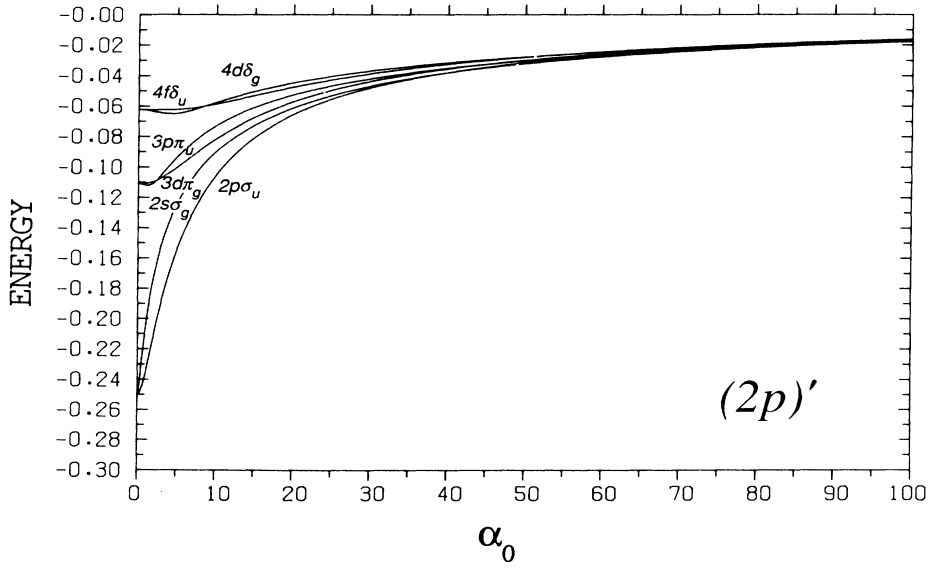

FIG. 8. The two families converging in the strong-field limit to the level $(2p)'$ for $n \leq 4$, as obtained from numerical calculation. Energies are expressed in Rydberg units.

ACKNOWLEDGMENTS

The author would like to thank Dr. M. Gavrila and Dr. N. R. Walet for interesting and stimulating discussions. This work was supported by Stichting voor Fundamenteel Onderzoek der Materie (FOM), which is a division of NWO, the Netherlands Organization for Scientific Research.

APPENDIX A: DERIVATION OF THE SCHRÖDINGER EQUATION IN TOROIDAL COORDINATES (η,θ,ϕ)

Expressing the Schrödinger equation, Eq. (1), in the toroidal coordinates (η,θ,ϕ) is most easily done, starting from Eq. (6), in which we have adopted the circular-cylindrical coordinates (ρ,z,ϕ).

We first cast Eq. (6) in the form

$$\left[-\frac{1}{2}\left[\frac{\partial^2}{\partial\rho^2}+\frac{\partial^2}{\partial z^2}-\frac{(m^2-\frac{1}{4})}{\rho^2}\right]-\frac{2}{\pi[(\rho+\alpha_0)^2+z^2]^{1/2}}K\left[\left[1-\frac{(\rho-\alpha_0)^2+z^2}{(\rho+\alpha_0)^2+z^2}\right]^{1/2}\right]\right]\bar{\Phi}(\rho,z)=E\bar{\Phi}(\rho,z)\ , \tag{A1}$$

where we have set

$$\bar{\Phi}(\rho,z)=\rho^{1/2}\Phi(\rho,z)\ . \tag{A2}$$

The transformation from circular-cylindrical coordinates to the toroidal coordinates, $(\rho,z)\rightarrow(\eta,\theta)$, as given by Eq. (9), can easily be shown to be orthogonal. Application of the standard expression for the Laplacian for such (two-dimensional) systems readily gives

$$\frac{\partial^3}{\partial\rho^2}+\frac{\partial^2}{\partial z^2}=\mathcal{S}^2\left[\frac{\partial^2}{\partial\eta^2}+\frac{\partial^2}{\partial\theta^2}\right]\ , \tag{A3}$$

with $\mathcal{S}$ given by Eq. (10).

Substitution of the expressions for ρ and z in terms of η and θ, as given by Eq. (9), yields for $[(\rho\pm\alpha_0)^2+z^2]^{1/2}$ $[=r_\pm$, see Eq. (4)],

$$r_\pm=\sqrt{2\alpha_0}e^{\pm\eta/2}\mathcal{S}^{-1/2}\ . \tag{A4}$$

Making use of the expression for ρ in Eqs. (9), (A3), and (A4) in Eq. (A1) then readily leads to the desired result, Eq. (11).

In order that the full wave function $\Psi(\rho,z,\phi)$ be normalized to unity we must have [see Eqs. (5) and (A2)]

$$\int_0^\infty\int_{-\infty}^{+\infty}|\bar{\Phi}(\rho,z)|^2d\rho\,dz=1\ . \tag{A5}$$

The Jacobian of the transformation of Eq. (9), $(\rho,z)\rightarrow(\eta,\theta)$, equals $\mathcal{S}^{-2}$. This yields for the normalization of $\bar{\Phi}(\eta,\theta)$

$$\int_0^\infty\int_{-\pi}^{+\pi}|\bar{\Phi}(\eta,\theta)|^2\mathcal{S}^{-2}d\eta\,d\theta=1\ . \tag{A6}$$

APPENDIX B: DERIVATION OF THE NEXT ORDER IN α_0^{-1} IN THE ASYMPTOTIC EXPRESSION FOR THE LEVEL ENERGY

In Sec. V we derived from Eq. (19) the expression, Eq. (30), for the energy of the levels in the high-α_0 limit. To find the next order in α_0^{-1}, we expand Eq. (19) through first order in μ:

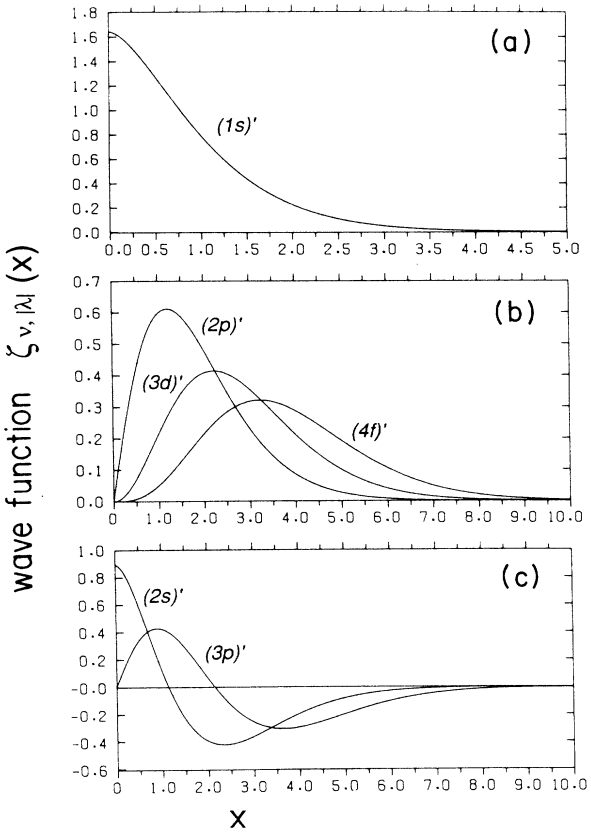

FIG. 9. Plots of $x^{-1/2}$ times the (normalized) solutions of the one-dimensional Schrödinger equation with a logarithmic potential, $\chi_{\nu,|\lambda|}(x)$ $[=\zeta_{\nu,|\lambda|}(x)]$ as given by Eq. (27) corresponding to the six lowest-energy eigenvalues $\varepsilon_{\nu,|\lambda|}$. (a) The state of lowest energy ($|\lambda|=0$, $\nu=1$). (b) The nodeless excited states for $|\lambda|=1$, 2, and 3. (c) The excited states having a single node for $|\lambda|=0$ and 1.

$$\left[-\frac{1}{2}\left[\frac{\partial^2}{\partial\xi^2}+\frac{1}{\xi}\frac{\partial}{\partial\xi}+\frac{1}{\xi^2}\frac{\partial^2}{\partial\theta^2}\right]+\ln\xi+\mu\xi\cos\theta(3\ln\xi-4\varepsilon_0-\ln\mu+2\ln 2)+O(\mu^2\ln\mu)\right]\phi_\mu(\xi,\theta)=\varepsilon_\mu\phi_\mu(\xi,\theta)\ . \tag{B1}$$

Since the full problem, Eq. (14), is invariant with respect to reflections in the xy plane, the perturbation vanishes to all orders between wave functions that are symmetric under the transformation $\theta\rightarrow-\theta$ and functions that are antisymmetric [to be specified by a superscript $(\pm)$].

Therefore Eq. (B1) can be solved up to order $\mu^2\ln\mu$, by applying first-order perturbation theory for nondegenerate states (the twofold degeneracy of levels with $|\lambda|\neq 0$ does not play a role), yielding

$$\varepsilon_\mu=\varepsilon_0+\mu\int_0^\infty\int_{-\pi}^{+\pi}|\phi_0^{(\pm)}(\xi,\theta)|^2\cos\theta(3\ln\xi-4\varepsilon_0-\ln\mu+2\ln 2)\xi^2 d\xi\, d\theta+O(\mu^2\ln^2\mu)\ . \tag{B2}$$

Note that the integral with respect to θ equals either

$$\int_{-\pi}^{\pi}\sin^2|\lambda|\theta\cos\theta\, d\theta\ ,$$

or

$$\int_{-\pi}^{\pi}\cos^2|\lambda|\theta\cos\theta\, d\theta\ ,$$

which is identically zero. We thus find that ε_μ equals ε_0 up to order $\mu^2\ln^2\mu$. The relations (20) and (21) thus show that expression (30) for $E(\alpha_0)$ is correct to order $\ln^2\alpha_0/\alpha_0^2$.

APPENDIX C: THE SCHRÖDINGER EQUATION WITH A LOGARITHMIC POTENTIAL

In this appendix we will discuss in some detail the solutions of the one-dimensional Schrödinger equation, Eq. (27).

The solutions of this equation can be expanded as[37]

$$\chi(x)=x^{|\lambda|+1/2}\sum_{m=0}^{\infty}\ln^m x\sum_{n=m}^{\infty}a_{mn}x^{2n}\ , \tag{C1}$$

the coefficients a_{mn} of which can be obtained from recurrence relations.

In Fig. 9 we have plotted $x^{-1/2}$ times the (normalized) wave functions $\chi_{\nu,|\lambda|}(x)$—which is the combination in which they appear in Eq. (29) and which we shall henceforth denote by $\zeta_{\nu,|\lambda|}$—corresponding to the six lowest-energy eigenvalues $\varepsilon_{\nu,|\lambda|}$ as obtained from numerical integration of Eq. (27). From Eq. (C1) we see that for x small $\zeta_{\nu,|\lambda|}(x)$ behaves as $x^{|\lambda|}$. This shows that for s' states, $\zeta_{\nu,|\lambda|}$ attains a finite value at $x=0$ in contrast to states other than those of s' type [see Fig. 9(a)]. It also explains why in Fig. 9(b) $\zeta_{\nu,|\lambda|}$ rises more slowly from the value zero for p', d', and f' states, respectively. Note that the maximum shifts to higher values of the argument as $|\lambda|$ increases, which is due to the term $|\lambda|^2/2x^2$ in Eq. (27), which acts as a centrifugal barrier and repels the particle from the origin. Figure 9 demonstrates that $\zeta_{\nu,|\lambda|}$ (for s' states) exhibits no cusp behavior as x tends to zero. Indeed, from Eq. (C1) it follows that the first derivative of $x^{-1/2}\chi_{\nu,|\lambda|}(x)$ vanishes if x tends to zero. Note, however, that the second derivative diverges logarithmically at zero. Numerical values for the eigenvalues $\varepsilon_{\nu,|\lambda|}$ for $\nu\leq 5$ and $|\lambda|\leq 4$ are given in Table I.

TABLE I. Eigenvalues $\varepsilon_{\nu,|\lambda|}$ of the logarithmic potential as determined by Eq. (27) for $|\lambda|\leq 4$ and $\nu\leq 5$.

ν \ $\lvert\lambda\rvert$	0	1	2	3	4
1	0.179 935				
2	1.314 678	1.039 613			
3	1.830 609	1.662 901	1.497 798		
4	2.168 875	2.047 765	1.929 288	1.811 273	
5	2.421 056	2.326 094	2.233 479	2.139 542	2.049 706

[1]Multiphoton ionization taking place by absorption of more than the minimum number of photons required to ionize the atom, was originally termed by Y. Gontier and M. Trahin [J. Phys. B **13**, 4383 (1980)] somewhat awkwardly "above-threshold ionization," which yields the acronym ATI. We will, however, prefer to use the more natural terminology "excess-photon ionization" (EPI).

[2]P. Agostini, F. Fabre, G. Mainfray, G. Petite, and N. K. Rahman, Phys. Rev. Lett. **42**, 1127 (1979).

[3]P. Kruit, J. Kimman, H. Muller, and M. van der Wiel, Phys. Rev. A **28**, 248 (1983).

[4]L.-A. Lompré, G. Mainfray, C. Manus, and J. Kupersztych, J. Phys. B **20**, 1009 (1987).

[5]H. Muller and A. Tip, Phys. Rev. A **30**, 3039 (1984); see also H. R. Reiss, Phys. Rev. A **22**, 1786 (1980).

[6]C. K. Rhodes, Science **229**, 1345 (1985).

[7]For recent advances, see, for example, *Ultrafast Phenomena VI*, edited by T. Yajima, K. Yoshihara, C. B. Harris, and S.

Shionoya (Springer-Verlag, Berlin, 1988), Pts. I and II.

[8]*Multiphoton Ionization of Atoms,* edited by S. J. Chin and P. Lambropoulos (Academic, New York, 1984).

[9]L. Pan, K. T. Taylor, and C. W. Clark, Phys. Rev. Lett. **61**, 2673 (1988).

[10]M. Gavrila and J. Z. Kaminski, Phys. Rev. Lett. **52**, 613 (1984).

[11]M. Gavrila, in *Fundamentals of Laser Atom Interactions,* Vol. 229 of *Lecture Notes in Physics,* edited by F. Ehlotzky (Springer, Berlin, 1986), p. 3.

[12]K. C. Kulander, Phys. Rev. Lett. **35**, 445 (1987). For an application to helium, solving the time-dependent Hartree-Fock equations, see K. C. Kulander, Phys. Rev. A **36**, 2726 (1987).

[13]M. Pont and M. Gavrila, Phys. Lett. A **123**, 469 (1987).

[14]R. R. Freeman, P. H. Bucksbaum, H. Milchberg, S. Darack, D. Schumacher, and M. E. Geusic, Phys. Rev. Lett. **59**, 1092 (1987).

[15]P. H. Bucksbaum, M. Bashkansky, R. R. Freeman, T. J. McIlrath, and L. F. Dimauro, Phys. Rev. Lett. **56**, 2590 (1986).

[16]M. Pont, M. J. Offerhaus, and M. Gavrila, Z. Phys. D **9**, 297 (1988).

[17]M. Pont, N. R. Walet, M. Gavrila, and C. W. McCurdy, Phys. Rev. Lett. **61**, 939 (1988). For a full account on the study of the lower-lying bound states for atomic hydrogen in the case of linearly polarized light, see M. Pont, N. R. Walet, and M. Gavrila, Phys. Rev. A (to be published).

[18]J. N. Bardsley and M. J. Comella, Phys. Rev. A **39**, 2252 (1989).

[19]R. Bhatt, B. Piraux, and K. Burnett, Phys. Rev. A **37**, 98 (1988).

[20]This condition can in fact be relaxed. Instead of the ground state one may take the state of lowest energy which is radiatively coupled to the initial state. For circular polarization, transitions between states of different parity with respect to a reflection in the polarization plane are inhibited. Thus one needs only consider the state of lowest energy with the same parity with respect to reflection in the polarization plane as the initial state.

[21]I. S. Gradshteyn and I. M. Ryzhik, *Table of Integrals, Series and Products* (Academic, New York, 1965).

[22]Implicitly we assume here the validity of the Wigner–von Neumann noncrossing rule [J. von Neumann and E. P. Wigner, Z. Phys. **30**, 467 (1929); L. D. Landau and E. M. Lifshitz, *Quantum Mechanics, Non-relativistic Theory* (Pergamon, New York, 1958), Sec. 76.] For the Hamiltonian of Eq. (6), which depends parametrically on m, it states that levels corresponding to states being either symmetric or antisymmetric with respect to reflection in the xy plane (i.e., transforming according to the same irreducible representation) do not cross as m is varied.

[23]Here we used the Feynman-Hellmann theorem [H. Hellman, *Einführung in die Quantenchemie* (Deuticke, Leipzig, 1937); R. P. Feynman, Phys. Rev. **56**, 340 (1939)] in its integral form. In differential form we have for a Hamiltonian H_λ, depending on some parameter λ and having a bound state ψ_λ with energy E_λ: $\partial E_\lambda/\partial\lambda=\langle\psi_\lambda|\partial H_\lambda/\partial\lambda|\psi_\lambda\rangle$. Integrating both sides gives $E_\lambda=E_0+\int_0^\lambda\langle\psi_{\lambda'}|\partial H_{\lambda'}/\partial\lambda'|\psi_{\lambda'}\rangle d\lambda'$.

[24]Note that $\langle\rho^{-2}\rangle_{|m|}$ does not exist for σ states, since they attain a finite value at the z axis. In general, the states $\Phi_{|m|}(\rho,z)$ will behave as $A_{|m|}(z)\rho^{|m|}$ for $\rho\downarrow 0$. Thus $\langle\rho^{-2}\rangle_{|m|}$ diverges as $|m|^{-1}$ as $|m|\downarrow 0$, the factor of proportionality being one-half times the integral $\int|A_0(z)|^2dz$, which is the probability density to find the electron in the σ state on the z axis. This does not lead to divergence of the integral of Eq. (7).

[25]P. Moon and D. E. Spencer, *Field Theory Handbook* (Springer-Verlag, Berlin, 1988).

[26]An elementary calculation from Eq. (9) and Eq. (13) yields $r=\hat{r}\mathcal{R}^{-1/2}$, $\sin\theta=\sin\hat{\theta}\mathcal{R}^{-1/2}$, with $\mathcal{R}=1+(\hat{r}/2\alpha_0)^2+2(\hat{r}/2\alpha_0)\cos\hat{\theta}$. Our statement then directly follows by noting that in the limit of close approach to the circle of charge ($\hat{r}\ll 2\alpha_0$) $\mathcal{R}$ tends to unity.

[27]To show this, we express the normalization integral of Eq. (17) in terms of our scaled quantities. This yields $\int_0^{2\alpha_0}\int_{-\pi}^{\pi}|\hat{\Phi}(r,\theta)|^2\mathcal{P}^{-2}r\,dr\,d\theta=\int_0^{\mu^{-1}}\int_{-\pi}^{\pi}|\phi_\mu(\xi,\theta)|^2\mathcal{P}^{-2}\xi\,d\xi\,d\theta$, from which Eq. (25) follows directly by taking the limit for $\mu\downarrow 0$ (i.e., $\alpha_0\rightarrow\infty$).

[28]In fact, it corresponds to it for $|\lambda|=l+\frac{1}{2}$, i.e., for half-integer values of l ($-\frac{1}{2},\frac{1}{2},\frac{3}{2},\ldots$).

[29]The normalization of the wave functions $\hat{\Phi}_{\nu,\lambda}(r,\theta)$, Eq. (31), can be easily verified by substitution of the expression Eq. (29). In the same way one can easily verify that Eqs. (29) and (30) satisfy the Schrödinger equation, Eq. (32).

[30]The fact that the levels converging to a main level $\nu|\lambda|$ constitute families can, apart from the energy position argument, also be seen as follows. For high α_0, according to Eq. (7), the influence of the centrifugal barrier becomes negligible and consequently the energy of the levels and the associated states $\Phi(\rho,z)$ of a family converge to each other (see the end of Sec. III). This is obviously the case for states converging to the same main level $\nu|\lambda|$, since as $\alpha_0\rightarrow\infty$ their energies become equal while they converge to the same function $\Phi(\rho,z)$ $[=\rho^{-1/2}\hat{\Phi}^{(\pm)}_{\nu,|\lambda|}(r,\theta)]$ which does not depend on m.

[31]We note that the wave function at high α_0 drops rapidly (i.e., exponentially) to zero if one moves away from the charged circle. The probability density to find the particle on the z axis for σ states is therefore exponentially small for high α_0 and the contribution of the singularity of $\langle\rho^{-2}\rangle_{|m|}$ as $|m|\downarrow 0$ (see Ref. 24) to the integral of Eq. (7) can thus be neglected.

[32]The operator associated with this transformation is $-i(\partial/\partial\theta)$. It allows us to look for the eigenfunctions of the full Schrödinger equation in the high-α_0 limit among those common to both this operator and $-i(\partial/\partial\phi)$.

[33]Thus we have chosen x_0 in Sec. VI equal to $\exp\varepsilon_{\nu,|\lambda|}$, which can be checked for being a reasonable choice by comparing this value making use of the data of Table I with the wave-function plots in Fig. 9 of Appendix C.

[34]Except those corresponding to half-planes through the z axis in case one takes the ϕ-dependent part $\cos(|m|\phi)$ or $\sin(|m|\phi)$, but these we will leave out of consideration; they stay unaltered by changes of α_0.

[35]In fact, the high-α_0 limit allows us to make statements about the wave function only in the vicinity of the charged circle. One should realize, however, that at high α_0 the wave function decreases rapidly to zero as one moves away from the circle, and the shape of the nodal surface is therefore only of interest near the circle of charge.

[36]It was found in Ref. 16 that the mean-square deviation from $\bar{r}$, Δr, also increases with α_0, though less rapidly than $\bar{r}$. The relationship found was linear for sufficiently high α_0. The present analysis shows that this quantity should in fact be proportional to the square root of α_0 rather that its first power. Obviously this deviation is a result of the approximate approach followed in Ref. 16.

[37]F. Gesztesy and L. Pittner, J. Phys. A **11**, 679 (1978).